Applied Materials Today 36 (2024) 102061

Contents lists available at ScienceDirect

Applied Materials Today

journal homepage: www.elsevier.com/locate/apmt

Artificial intelligence generates novel 3D printing formulations

Moe Elbadawi [a], Hanxiang Li [b], Siyuan Sun [b], Manal E. Alkahtani [b,c], Abdul W. Basit [b], Simon Gaisford [b,*]

[a] School of Biological and Behavioural Sciences, Queen Mary University of London, Mile End Road, London E1 4DQ, UK
[b] UCL School of Pharmacy, University College London, 29-39 Brunswick Square, London WC1N 1AX, UK
[c] Department of Pharmaceutics, College of Pharmacy, Prince Sattam bin Abdulaziz University, Alkharj 11942, Saudi Arabia

ARTICLE INFO

Keywords:
Machine learning
Neural networks
Deep learning
Generative AI
Additive manufacturing
Drug delivery and drug development
Big data

ABSTRACT

Formulation development is a critical step in the development of medicines. The process requires human creativity, ingenuity and in-depth knowledge of formulation development and processing optimization, which can be time-consuming. Herein, we tested the ability of artificial intelligence (AI) to create *de novo* formulations for three-dimensional (3D) printing. Specifically, conditional generative adversarial networks (cGANs), which are generative models known for their creativity, were trained on a dataset consisting of 1437 fused deposition modelling (FDM) printed formulations that were extracted from both the literature and in-house data. In total, 27 different cGANs architectures were explored with varying *learning rate, batch size* and *number of hidden layers* parameters to generate 270 formulations. After a comparison between the characteristics of AI-generated and human-generated formulations, it was discovered that cGANs with a medium *learning rate* (10^{-4}) could strike a balance in generating formulations that are both novel and realistic. Four of these formulations were fabricated using an FDM printer, of which the first AI-generated formulation was successfully printed. Our study represents a milestone, highlighting the capacity of AI to undertake creative tasks and its potential to revolutionize the drug development process.

1. Introduction

Three-dimensional (3D) printing, also known as additive manufacturing, has emerged as a disruptive technology with the potential to revolutionise various industries, including energy, aerospace and pharmaceutics [1–7]. In healthcare, its ability to fabricate complex 3D structures with precision and customisation holds immense promise for advancing medicines [8–10]. 3D printing enables the production of both precision and personalised medicines, tailored to individual patients' needs, thereby improving therapeutic efficacy and patient outcomes [11,12]. However, despite its enormous potential, 3D printing of medicines is still in its infancy and lags behind other established technologies. Realising the potential of 3D printed medicines will require an exhaustive research endeavour that will be both time- and cost-intensive.

To advance developments in the field, *in* silico tools have been adopted to achieve progress in a rapid and sustainable manner. Artificial intelligence (AI) has emerged as a transformative *in silico* tool across various scientific disciplines, and its potential to enhance 3D printing technology in pharmaceuticals is increasingly recognised [13–15]. The overarching aim of AI is to replicate human intelligence such that machines can perform tasks, including those deemed complex or dangerous [16–21]. At its core, AI is trained on data and its parameters are optimised such that AI learns to perform tasks optimally [22]. A unique selling point of AI is its ability to handle large and complex datasets. Moreover, AI can comprehend data of different formats, such as numeric and text. These features collectively allow AI to work towards replicating human intelligence.

In material synthesis and processing, AI technologies have been applied to accelerate developments, including predicting formulation processability, real-time quality control of dosage forms and elucidating drug interactions [23–32]. Such applications typically involve training models to learn patterns and make predictions based on labelled data. These models excel at tasks such as classification and regression. However, when it comes to generating new data, traditional ML methods face limitations.

This is where Generative Adversarial Networks (GANs) distinguish themselves. Unlike traditional ML, GANs consist of two competing

* Corresponding author.
E-mail address: s.gaisford@ucl.ac.uk (S. Gaisford).

https://doi.org/10.1016/j.apmt.2024.102061
Received 7 November 2023; Received in revised form 3 January 2024; Accepted 5 January 2024
Available online 13 January 2024

components: a Generator and a Discriminator. The Generator learns to generate synthetic data samples that closely resemble the training data, while the Discriminator evaluates the authenticity of these samples. Through a continuous adversarial learning process, GANs excel at generating new and realistic data, capturing intricate patterns and producing diverse outputs [33]. In other words, GANs are like a student and a professor working together to replicate work from a published study. The student is the Generator that generates the data, while the professor is the Discriminator, evaluating the quality of the data. The student and the professor work together iteratively until the professor is satisfied with the quality of the data generated by the student. Eventually, the quality of the student's work becomes so good that they can start exploring their own research. GANs use this unique partnership to generate new and exciting content, whether it's realistic images, music, or even new drugs [34–38]; previously believed to tasks only achievable by humans.

GANs have gained significant attention in recent years due to their ability to generate realistic and diverse data in a number of fields, including material science and medicine [33,39–42]. In the context of drug discovery, GANs offer several distinct advantages over traditional ML techniques. GANs can capture complex, high-dimensional data distributions, enabling the generation of novel drugs with desired properties, such as enhanced solubility [43–47]. By training on large datasets of compounds with known biological targets and associated properties, GANs can learn to navigate the vast chemical space and propose novel candidates that meet specific design criteria. They have been employed to generate diverse chemical structures, optimise drug-like properties, predict biological activities, and generate novel materials [37,48–55]. The application of GANs in both drug discovery and material synthesis has shown promising results in generating new material entities with desired properties, thereby expediting developments in a sustainable manner. However, the use of GANs later in the formulation process has yet to be explored. Material processing is a complex step that involves optimising both the admixture and the processing parameters, resulting in a large search space. For medicines, the complexity increases as excipients, also referred to as additives, are functionalised with the addition of a drug, and thus need to be compatible with one another. Moreover, all components of a medicine – both excipients and drugs – have to be biocompatible and meet high regulatory standards. Hence the slow advancements in pharmaceutical formulation development.

In this paper, we harness the potential of GANs to elucidate whether AI can generate new fused deposition modelling (FDM) formulations. We present a novel framework that leverages GANs to generate new pharmaceutical formulations optimised for FDM, and by extension polymeric hot melt extrusion (HME), that have been functionalised with an active pharmaceutical ingredient (API). We compare the AI-generated formulations with human-generated FDM formulations. Through this innovative approach, we aim to advance the field of 3D printing in drug development by expanding the FDM formulation space rapidly and sustainably, and contribute to the realization of personalized medicine.

2. Results

In total, 1437 formulations, containing 336 pharmaceutical-grade materials, were used for model training, all of which had been generated by (human) researchers in the field. The training dataset was cleaned and pre-processed and then fed into the conditional GANs (cGANs). For this application, cGANs were selected over regular GANs to help improve the probability of the model outputting printable formulations. Fortunately, the dataset was already labelled with the printability outcome of each of the 1437 formulations, which allowed us to use supervised cGAN architectures. cGANs allow the architecture to be conditioned on which formulations are printable and which are not printable. Hence, this added conditional feature allowed the model to generate not only formulations but also FDM-printable formulations. Thus, the cGAN models were fed both the formulation composition and their respective printability outcome (i.e., 'Yes' for printable; 'No' for unprintable). The cGANs was then conditioned to generate new printable formulations (Fig. 1).

2.1. Model training

In this preliminary study, a three-level factorial framework was developed to investigate three important cGAN parameters; the *learning rate*, the *batch size* and the *number of hidden layers* in the Generator (Table S1–1). These three factors are known to influence the performance of the overall GAN, and their effect was determined by the complexity of the task and the training dataset.

The loss values for each model were recorded, which provided insight into a model's learning behaviour. These can be interpreted like other loss curves for neural networks, in which lower values indicate better performance of the model. However, since cGANs, as mentioned in the Introduction, are comprised of two competing neural networks, a decreasing loss value in one network will indicate that one-half of the model is improving, but it should not improve to the extent that it jeopardises the other's learning. For example, a decreasing loss value for the Discriminator will indicate that the Discriminator is improving in distinguishing between real and fake formulations, however, too much of an improvement will mean that the Discriminator will only accept formulations generated by the Generator that are identical to those found in the training dataset. Thus, a balance is needed between the two networks with regards to their learning behaviour.

Sample loss curves are shown in Fig. 2, while all the loss curves are provided in the supplementary information (Figs. S1–1, S1–2 and S1–3). These curves illustrate the loss values for both the Generator and the Discriminator. All models were allowed to train for 1000 epochs (i.e., feedback iterations), which helped in optimising the performance of both the Generator and Discriminator. The first nine sets of experiment were centred on keeping the learning rate at a constant 10^{-2}, whilst investigating different Generator hidden layers and batch size. For all nine architectures, a sudden decrease in Discriminator loss value was observed that subsequently plateaued and eventually reached zero. Conversely, a sudden increase in the Generator's loss value was observed, from approximately 8 to 15, which also plateaued, albeit oscillating throughout. The next set of nine experiments were based on a learning rate of 10^{-4}, while varying the Generator's hidden layer and model batch size. A lower learning rate is associated with better learning but at a slower pace. The process is analogous to that of reading a book: slowly reading a book can allow you to gain more information about the book's content, but it will demand more time. For these sets of architectures, both loss curves remained constant and oscillated around their initial value. The Generator and Discriminator loss values at 1000 epochs ranged between 9.05–10.54 and 0.28–1.24, respectively.

The last set of nine experiments involved further decreasing the learning rate to 10^{-6}, whilst similarly varying the Generator hidden layers and model batch size. These architectures presented similar loss curves to those of Models 10–18. The Generator and Discriminator loss values at 1000 epochs ranged between 7.66–10.07 and 1.34–1.38, respectively. Thus, while the loss value ranges overlapped with the Models 10–18, the Discriminator values were always greater. Overall, the cGANs performance was largely governed by the learning rate. Varying the Generator's hidden layers or varying the batch size had minor influence on both the Generator and Discriminator loss curves. Hence, irrespective of these two parameters, every model within a given *learning rate* produced comparable loss curves.

2.2. Comparing AI-generated to human-generated formulations

While the ability of AI to generate formulations is itself impressive, it would be more impactful if these formulations suggested were indeed novel, because this would both expand the FDM formulation space and

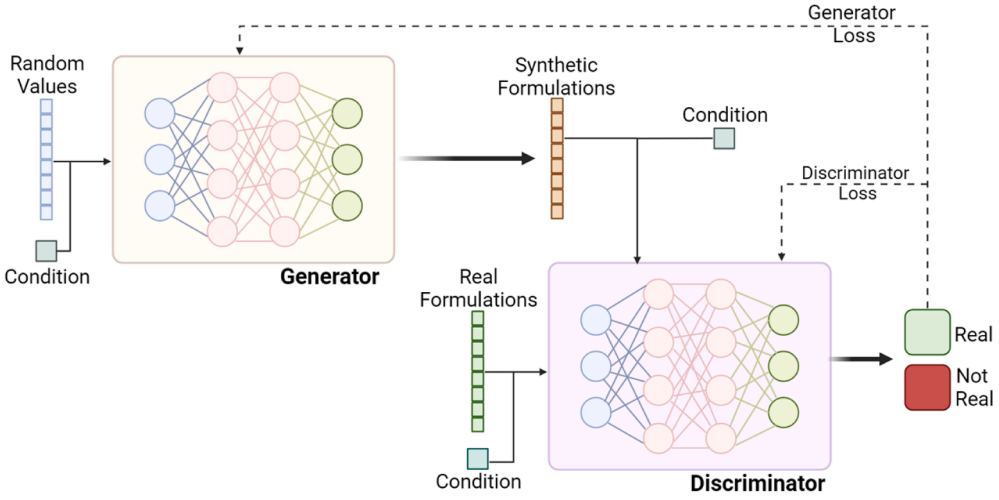

Fig. 1. Schematic depicting the cGANs. The model consisted of two neural network architectures (Generator and Discriminator) that are competing with each other. The Generator begins from a random distribution of numbers to output what it thinks are formulations. These synthetic formulations are fed into the Discriminator, having been also trained on the training dataset comprising real formulations. This helps the Discriminator to distinguish between randomly generated values and real formulations. The process is iterated, with each iteration helping the Generator improve its abilities in generating synthetic formulations that are more realistic to human-generated formulations.

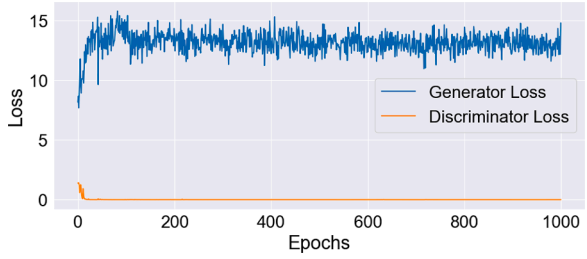

Fig. 2. An example of a loss curve from a model trained with a learning rate of 10^{-2}. The loss curves were used to determine model performance.

potentially address unmet clinical needs. Each model was instructed to generate ten printable formulations, resulting in a total of 270 formulations. A novel formulation is defined as one that does not exist in the training dataset. In other words, the AI-generated formulations should not be duplicates of formulation from the training dataset.

Comparing the AI-generated formulations with the training dataset (i.e., human-generated formulations) revealed that novel formulations were indeed generated by some of the models (Fig. 3(A)). Models 1–9 generated non-novel formulations. Further inspection of the generated formulations revealed that collectively, Models 1–9 generated identical formulations. Specifically, Models 1–4 and 6–9 duplicated the same formulation (Fig. 3(B)), whilst Model 5 duplicated the same formulation 9 times. Models 1–9 had a fast learning rate that resulted in the lowest Discriminator loss, with all models achieving zero Discriminator loss after 1000 iterations. Low Discriminator losses, particularly zero, mean that the Discriminator has perfectly learnt the dataset to the extent that it would be difficult for it to be tricked by the Generator [56–60]. It was thus evident that for Models 1–9, their respective Discriminator would only accept formulations if they already existed in the training dataset. Consequently, it can be concluded that Discriminator losses were significantly low enough that they were unable to generate novel formulations.

In contrast, Models 10–18 and Models 19–27 were able to generate novel formulations with either 9/10 or 10/10 formulations being novel (Fig. 3(A)). These models presented with a larger Discriminator value compared to Models 1–9, which were large enough to generate novel formulations. Further inspection revealed that two models from each set generated duplicate formulations, with Model 15 generating 6 duplicates, Models 18 and 25 generating 5 duplicates each and Model 22 generated only 2 duplicates. In total, Models 1–9, 10–18 and 19–27 generated 0 %, 84 %, 93 % novel formulations, respectively.

Having successfully demonstrated that the cGANs were capable of generating novel formulations, we then assessed their characteristics with respect to existing formulations, to determine whether they could capture the characteristics of how researchers formulate FDM formulations. One such characteristic was the number of materials (i.e., components) used per formulation. The training dataset consisted of formulations comprised of anywhere between 1 and 7 materials per formulation, with a median of 3 materials per formulations (Fig. 4). A common 3-material formulation consisted of a polymer, a lubricant and an API.

Models 1–9 (i.e., with the high learning rate) were found to generate one material per formulation, hence they were single-material formulations (Fig. 5). Models 10–18 on average generated formulations with a median between 1.7 to 12.3 materials per formulations, with the exception of Model 17 that exhibited a high median value. Models 19–27 generated, on average, a larger number of materials per formulation, with a median range of 18.3 to 51.0 materials per formulation, with the exception of Model 25, which had a median of 1.9 materials per formulation. Therefore, the majority of formulations generated by the low learning rate of 10^{-6} greatly exceeded the number of materials per formulation compared with the training dataset. On the other hand, Models 1–9 and 10–18, with the exception of Model 17, generated formulations that were more reflective of the training dataset with regards to the number of materials used per formulation.

In addition to generating API-loaded formulations, the amount of API was also inspected for the models that contained APIs. In the training dataset, the API content for the API-loaded formulations ranged between 0.25 and 60 w/w%, with a median value of 14 w/w% (Fig. 7(A)). The points in the scattered box-plot (Fig. 7(A)) provide insight into human-generated formulations, where it can be seen that numerous scatter points occupy the same value. It illustrates that most human-generated formulations favour API amounts with a round number (e.g., 20, 30 and 40 w/w%). In comparison, Models 10–18 and 19–27 presented with an API amount that ranged between 0.57 to 100 w/w%, with a mean value of 5.79 w/w%, as portrayed in Fig. 7(B). Thus, with regards to API loading, there is clear overlap between the AI-generated formulations to those from the training dataset. Interestingly, the formulations that contained the highest drug loading from both datasets (i.

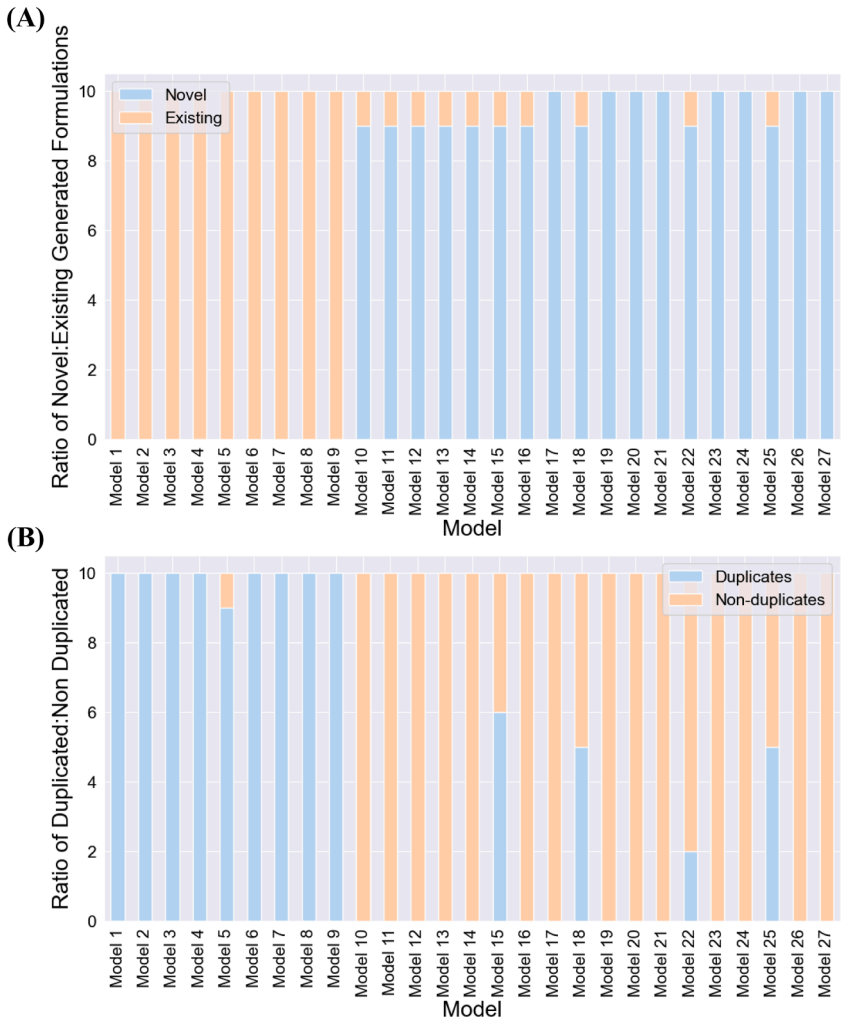

Fig. 3. Bar graphs highlighting the number of duplicates found in each model. Each model architecture was tasked to output 10 formulations, where (A) highlights whether the generated formulations are indeed novel or duplicates of formulations from the existing training dataset. It was found that some models learned to generate the same formulation and (B) depicts how many of the 10 formulations are duplicates of each other.

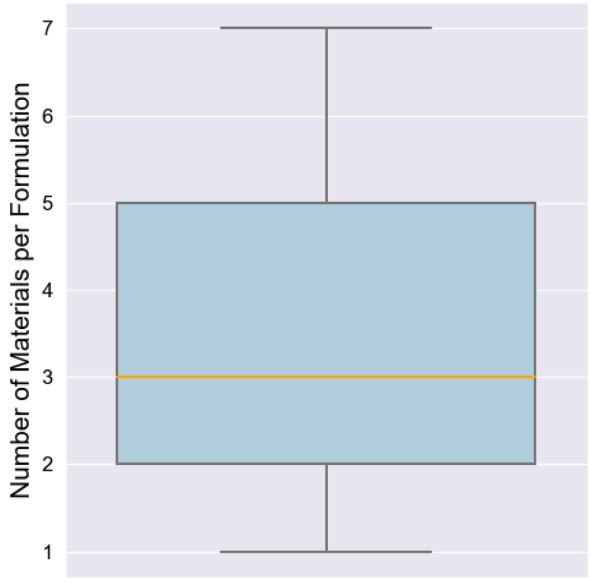

Fig. 4. Box-plot depicting the range of materials used per formulation.

e., 100 w/w% for the AI-generated and 62 w/w% for the training dataset) contained the same drug, isoniazid.

The AI-generated formulations' physical properties were analysed and compared with formulations from the training dataset. Compared with the previous characteristics, such as number of materials per formulation, physical properties provide more fundamental information about a formulation's characteristics, especially since parameters like molecular weight and melting point have been demonstrated to influence FDM printability [61,62]. Sixteen different features (Table S1–2) were used to represent both the original and AI-generated formulations, and the features were centred around the mwt, T_m and T_g of the materials within the formation. Principal component analysis (PCA) was used to decompose the sixteen dimensions to two for easy visual inspection (Fig. 8), effectively producing a two-dimensional space that mapped the FDM formulation space. In essence, points closely situated indicate similar formulations while points further apart represent more distinct formulations, in terms of physical property characteristics.

Within the FDM formulation space, the formulations from the training dataset were largely found in the centre and stretched into both the positive principal component (PC) 1 and positive PC2 space, and in the negative PC1 direction to a lesser extent. In comparison, the AI-generated formulations occupied similar areas within the formulation space, as well as areas far removed from the human-generated formulations. It can be seen that the AI-generated formulations expanded the

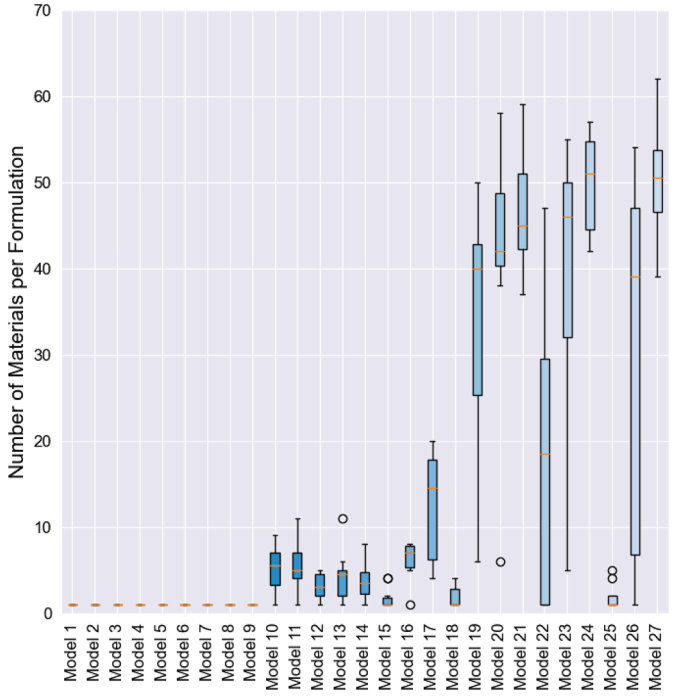

Fig. 5. Box-plots depicting the distribution of the number of materials used per formulation. Models 1–9 generated single-material formulations. Models 10–18 generated a realistic number of formulations, whereas Models 19–27 were found to sometimes generate formulations with a large number of materials.

FDM formulation space largely in the positive PC1 direction and in both the positive and negative PC2 directions. Occupying areas distinct from human-generated formulations indicates novel formulations, with respect to physical properties.

Models 1–9 shared identical regions with formulations from the training dataset, which is understandable since these were duplicates of existing formulations. Formulations belonging to Models 10–18 and 19–27 were found to spread out more, and can be seen to occupy regions distant from the training dataset formulations. Examples of these distant clusters belonging to Models 10–18 were observed around coordinates (3,−3), and clusters for Models 19–27 were observed around coordinates (12,−5). Models 19–27 were also observed to generate novel formulations that clustered near the training dataset formulations, at around (4,1.25). Overall, the results revealed that the AI-generated formulations occupied different regions of the formulation space, which is further indicative of generating novel formulations.

In summary, altering the *learning rate* of cGANs resulted in the generation of a range of formulations with diverse characteristics. Models developed with a learning rate of 10^{-2} generated formulations that were either identical to formulations in the training dataset or were less valuable as they contained no API. On the other hand, models with a learning rate of 10^{-6} were able to generate novel formulations that were (i) not replicates of formulations from the training dataset; and (ii) occupied regions in the formulation space distinct from the training dataset. However, these models tended to generate formulations with unrealistic characteristics; for example, containing up to 93 different APIs in a single formulation. cGANs with a learning rate of 10^{-4} tended to generate novel formulations and were more reflective of human-generated FDM formulations.

2.3. Experimental results

Four AI-generated FDM formulations were tested in order to validate the generative model experimentally. All four formulations were generated by Models 10–18, as this model set was capable of generating formulations that were novel and appeared realistic, according to the results from the previous section. The four formulations were located in the PCA plot around coordinates (3,−3). The compositions of the formulations are presented in Table 1. These four formulations comprised of different compositions but shared common traits, such as a main polymer of Klucel® EF, which is a hydroxypropylcellulose. Moreover, all contained the same API, paracetamol. The evident differences between all four formulations were the material components included and their respective mass fractions.

The formulations were prepared using a pestle and mortar, and subsequently processed by HME to generate the filament needed for FDM. All four formulations extruded well and resulted in filaments with diameter of 1.75 ± 0.1 mm (Fig. 9(A)). When printing, all four formulations possessed the ideal semi-molten properties and were extruded through the FDM nozzle, with medicinal tablets being printed (Fig. 9 (B)). In particular, Formulations 3 and 4 produced whole tablets. Therefore, we demonstrate that AI is not only capable of generating theoretical FDM formulations but also actual *de novo* formulations. Physicochemical analysis was performed to monitor all four formulations throughout the processing stages, and the results are presented in Supplementary 2.

3. Discussions

The study successfully demonstrates the utility of AI for generating *de novo* 3D printing formulations, thereby demonstrating that AI has the creativity to generate new pharmaceutically-functionalised formulations. This is a significant milestone in formulation development because to date, creating new formulations has been accomplished through human creativity. Researchers generate new formulations through structured scientific methods, which involves critically evaluating data, forming hypotheses and iterating based on empirical results [63]. This step-by-step process allows researchers to formulate new ideas based on existing scientific knowledge, intuition, or experience. Some are fortunate to have a “eureka” moment, but the creativity process is no easy feat [64]. If creativity can be automated with AI, and with AI’s ability to interpret large volumes of data and of different formats rapidly, then there is the prospect of accelerating developments in pharmaceutics through developing new innovative formulations. Other AI applications in pharmaceutics have demonstrated the potential for the technology to replace human tasks, such as predicting whether a formulation will work or inspecting the quality of dosage forms [28,62,65]. The present study demonstrates that AI has the potential to replace another human task – creativity – arguably the hardest task due to its subjective and complex nature. In other fields, this is indeed the vision sought for Generative AI.

As this was the first study, and to help with managing the data analysis, relatively few cGAN parameters were explored. In addition, the number of different parameter ranges were also kept small (i.e., 3 different values per parameter) and the number of formulations generated per model was kept to 10. It would have been easy and quick to task the model to generate 1000 formulations per model for instance, but this would have been overwhelming to interpret. Even generating 270 formulations in total was challenging to interpret, which is why we adopted a methodological approach to filtering out non-novel and unrealistic formulations. Evidently, it was possible for cGANs to generate a range of different formulations, however, a thorough characteristic comparison was needed to identify which of the 270 formulations were indeed both novel and realistic of human-generated formulations. Hence the evaluation pipeline, which included comparing the number of materials per formulation, duplicates and inspecting the FDM formulation space, was sufficient to evaluate the AI-generated formulations with regards to novelty and realism (Figs. 4–9). Furthermore, it is also worth noting that despite developing a relatively small cGAN architectures, they were sufficient in generating printable *de novo* formulations from a relatively small dataset of 1437 instances.

Table 1
AI-generated formulations used to experimentally validate the model. The table also includes the processing parameters used to generate the filament and FDM print. All formulations were FDM printed with a nozzle temperature of 180 °C.

Formulation	Materials	Composition (w/w%)	HME temperature (°C)	HME Nozzle Size (mm)	3D Printing Nozzle Size(mm)
Formulation 1	Klucel® EF	72.520	85	1.5	1.6, 1.8
	Paracetamol	11.34			
	Mannitol	5.174			
	Magnesium Stearate	4.614			
	Aquasolve® LG	4.210			
	Natrosol™ 250H	2.142			
Formulation 2	Klucel® EF	58.600	77	1.4	1.6, 1.8
	Paracetamol	23.720			
	Natrosol™ 250H	6.120			
	Polyox™ WSR 303	6.000			
	Mannitol	5.000			
	Aquasolve® HG	0.560			
Formulation 3	Klucel® EF	74.400	100	1.3	1.6
	Mannitol	14.920			
	PEO 8M	5.320			
	Magnesium Stearate	4.260			
	Paracetamol	1.100			
Formulation 4	Klucel® EF	83.200	95	1.4	1.6
	PEO 8M	4.190			
	Natrosol™ 250H	3.740			
	Paracetamol	2.640			
	Magnesium stearate	2.420			
	Mannitol	2.340			
	PEG 8K	0.930			
	Kolliphor® 407	0.540			

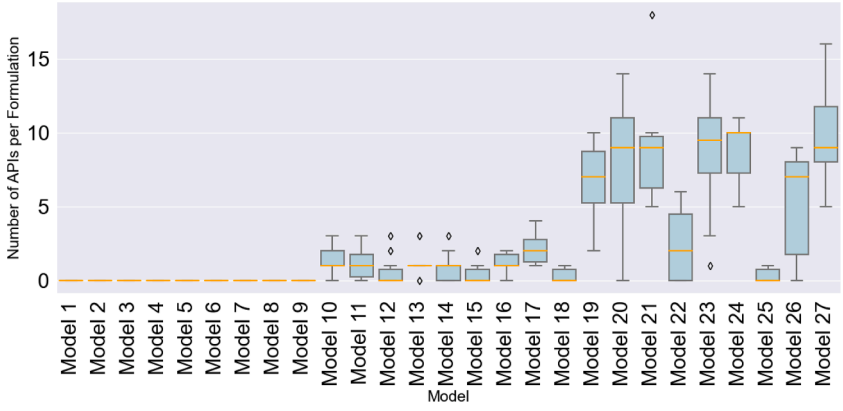

Fig. 6. The average number of APIs per formulation. Models 1–9 generated formulations containing no API, whilst Models 19–27 generated some formulations containing more than 10 APIs. Models 9–18 appeared to generate formulations with a more reasonable number of APIs per formulation.

It was apparent that one parameter, *learning rate*, can impact the quality of generated data [56]. cGAN architectures built using higher *learning rate* generated formulations identical to formulations in the training dataset and lacked diversity. High learning rates can lead to faster model training times, however, they have been reported to produce deteriorating results due to model overfitting, which can manifest in the Generator memorising data from the training dataset [66–73]. This was evident as *learning rate* of 10^{-2} produced the lowest Discriminator loss values. Therefore, for this application, a learning rate 10^{-2} appeared to be high. A subsequent analysis revealed that a learning rate of 10^{-1} also resulted in model overfitting (data not included).

Low learning rates of 10^{-6} were found to generate unrealistic formulations, with formulations containing a large number of different APIs in one formulation. On the other hand, the medium learning rate struck a good balance between convergence and stability during training needed for the cGANs to capture the underlying data distribution more effectively. These results highlight the crucial role of the *learning rate* in cGAN training, with a medium *learning rate* of 10^{-4} demonstrating improved performance in generating new formulations with the current dataset. Therefore, the results suggest that with hyper-parameter tuning, there is potential for cGANs to generate more *de novo* formulations from a relatively small dataset of 1437 formulations. This means that cGANs can be used at the early stages of a technologies life cycle to realise its formulation space, and what it can and cannot fabricate.

We validated formulations generated by cGAN architectures trained using the medium *learning rate* experimentally to determine the reliability of the models. The four formulations were all extrudable by both HME and FDM, but only two of the formulations were found to print successfully complete tablets. We believe that with further modifications to our bespoke printer, all four could have been completely printed. FDM printers are available in different forms, such as direct-drive or Bowden extrusion, which means that without the same FDM setup it can be hard to replicate published work. The same can also be extended to Generative AI models trained on literature-extracted formulations. While literature-extraction can lead to an increase in dataset size, there is the possibility that AI models can predict/generate formulations that are not compatible with some FDM printers.

Interestingly, the formulations tested all contained Klucel® EF as the polymer base. This polymer was explored in earlier FDM publications and still continues to be used in more recent publications [74,75].

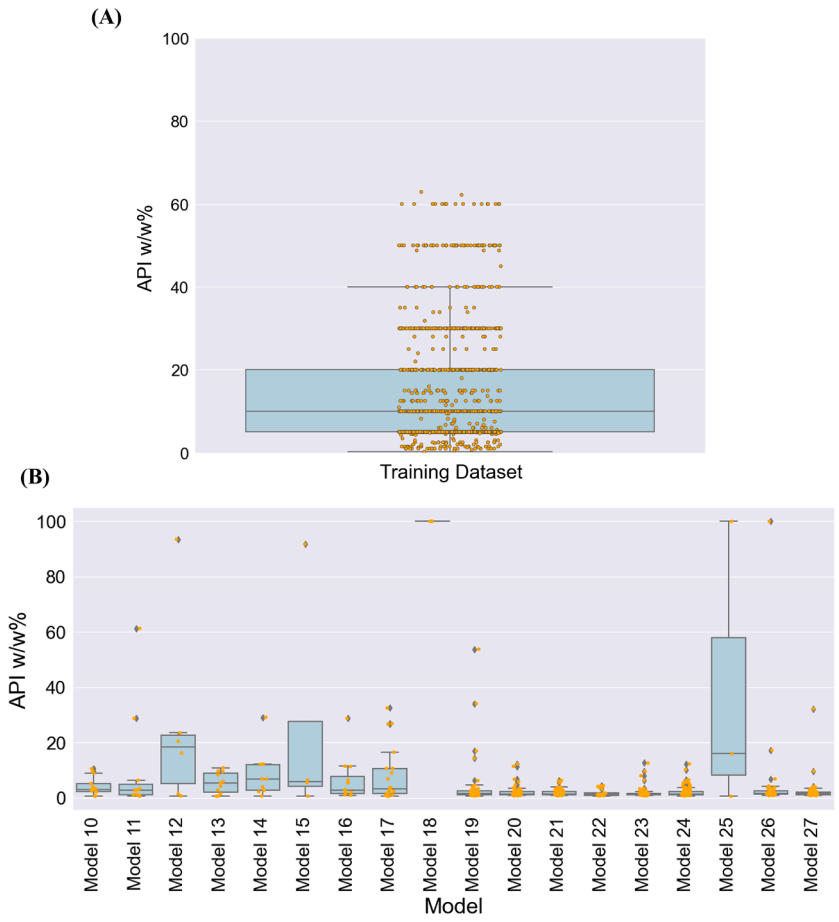

Fig. 7. A scattered box-plot depicting the distribution of drug w/w% in (A) the training dataset and (B) the AI Generated Formulations for Models 10–27, which contained an API.

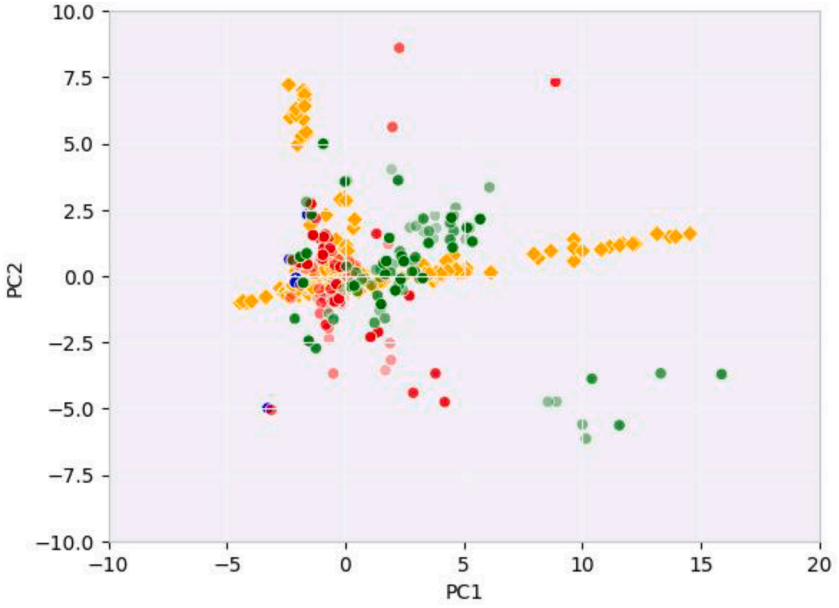

Fig. 8. A two-dimensional representation of the physical properties space for the FDM formulations. The original formulations are represented by orange diamonds, whereas the circles represent the AI generated formulations. Models 1–9 are in blue circles. Models 10–18 are in red circles and Models 19–27 are in green circles.

Therefore, it is clearly of interest to pharmaceutical 3D printing. It is possible that the number of formulations in the training dataset containing this polymer may have influenced the model. In other words, the model may have been biased towards Klucel® EF as it was used in 132 of the 1437 formulations. Only a few components were used more than Klucel® EF; either APIs (paracetamol and theophylline), plasticizers

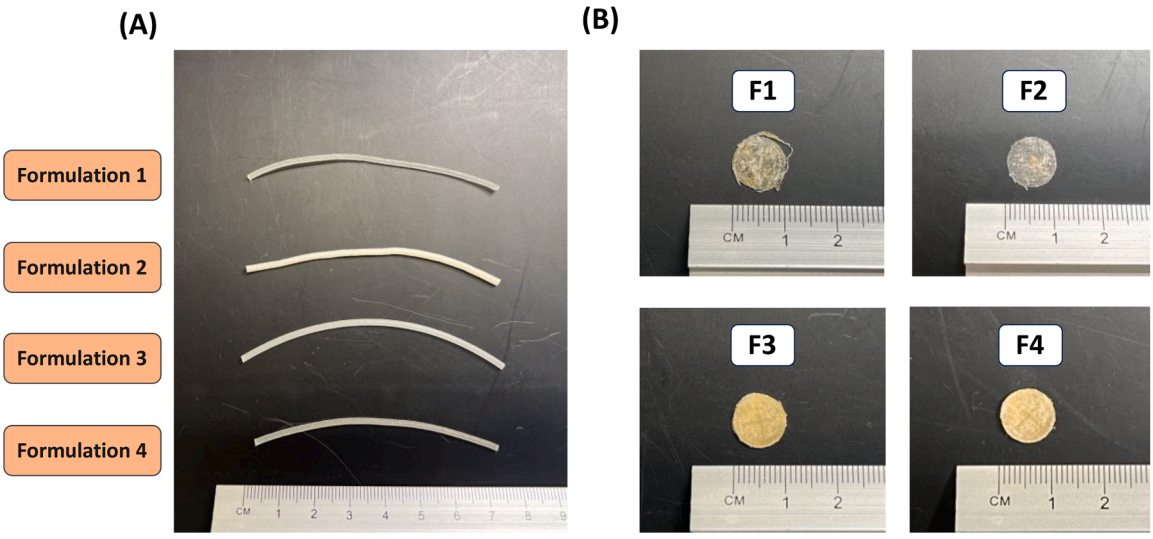

Fig. 9. The AI-generated (A) HME filaments and (B) FDM-printed tablets. All four AI-generated formulations were successfully processed into filaments, whereas 2/4 formulations (F3 and F4) were printable by FDM.

(triethyl citrate and mannitol) or a lubricant (magnesium stearate). Incidentally, paracetamol and mannitol were found in all four formulations, with magnesium stearate in three. It is possible that these models were biased towards the more frequently used components, where model bias is an issue affecting many black-box models [76,77]. Nevertheless, the novel compositions of all four formulations have expanded the FDM formulation space (Fig. 8), and will help guide future formulation development by highlighting new, printable regions in the FDM formulation space. Moreover, the ability of the cGAN architecture to recognise that Klucel® EF should be the dominant component means that it was able to capture the nuance of FDM formulations.

Moving forward, there are a number of potential research avenues to explore with generative models. The present study was a preliminary demonstration of its potential to create new formulation. Future work should seek a more targeted unmet need. For example, generative models should be tasked with creating a formulation for treating cancers or diabetes. Another possibility is the development of a Generative model that can predict more than one facet. For example, the filament mechanical properties are known to influence printing, and thus a more pragmatic Generative model should be able to predict not just the printability but also the filament mechanical properties. Furthermore, there are a number of other Generative AI models that can be explored [78].

In summary, we successfully demonstrated that generative models have the potential creativity to generate *de novo* FDM formulations using cGANs. A training dataset of 1437 FDM formulations that were extracted from an in-house database and the scientific literature were used to train 27 different cGAN architectures, with varying combinations of *learning rate, batch size* and *number of hidden layers*. A thorough analysis of formulation characteristics revealed that the cGANs can generate a range of formulations, but some already existed in the training dataset and some generated unrealistic formulations, such as those including a large number of APIs in one formulation. A *learning rate* of 10^{-4} was found to generate both novel and more realistic formulations. After inspecting the FDM formulation space, 4 formulations generated by cGANs were experimentally tested. The experimental test revealed that all were capable of forming filaments with ideal dimensions, and medicinal tablets of varying qualities were printed. Therefore, the experimental validation demonstrated that our cGAN methodology was capable of generating real *de novo* FDM formulations. Future work will seek to build on this study and use Generative AI models for targeted formulation development. The ideal Generative AI model should be able to both generate novel formulations and capture realistic formulation characteristics.

4. Methods

4.1. Data collection

The formulation dataset was a combination of in-house and literature-extracted data. A detailed description of the data collection, structure and labelling is provided in Refs. [79,80]. The dataset consisted of the composition of formulations and whether they were printable or not. The dataset was cleaned to remove any incomplete formulation data. In total, 1437 formulations from 336 different combinations of materials were used for training.

4.2. Model development

For this study, conditional GANs (cGANs) were used. cGAN architectures were developed using Python (v.3.10.12), TensorFlow (v.2.0.0) and scikit-learn (v.0.24.2) packages. First, the printability feature, which was either a 'Yes' or 'No', was label encoded into a binary output of (0,1). A total of 27 different cGAN architectures were explored with varying *learning rate, batch size* and *number of hidden layers* for the Generator, as enumerated in Table S1–1. The remaining parameters were kept constant, which for the Generator were the number of neurons for the input layer (150), the number of neurons per hidden layer (512) and the activation function (*relu*), the number of neurons for the output layer (336) and the activation function (*Softmax*). For the Discriminator, the parameters kept constant were the number of neurons per input layer (336), the number of hidden layers (2), the number of neurons per hidden layer (512) with an activation function (*relu*) and a dropout rate of (0.4), the number of neurons for the output layer (1) and an activation function (*Sigmoid*). The loss function (*binary cross entropy*), the optimiser (*Adam optimiser*), and the input layers and epoch (1000) were also kept constant.

Preliminary cGAN models were found sometimes to generate formulations that totalled anywhere between 90 and 105 w/w%. Thus, a post-processing normalising step was implemented to ensure that the formulation composition totalled 100 w/w%. The step involved first calculating the total sum for each generated formulation and dividing each component within the formulation by the total sum. This resulted in the components being scaled such that the total for each formulation summed to 100 w/w%, and were hence realistic of FDM formulations.

4.3. Formulation physical properties space

The formulation physical properties space was generated from a total 16 features centred on the molecular weight (mwt), glass transition temperature (T_g) and melting temperature (T_m). Three of the features pertained to the weighted mwt, T_g and T_m as previously described[80]. Briefly, the physical property was represented as the average of all the components in a formulation, but weighted by the proportion of the material present in the formulation. For example, the weighted mwt for a formulation comprising 3 materials is:

$$mwt_w = \frac{(w_1 + mwt_1) + (w_2 + mwt_2) + (w_3 + mwt_3)}{w_1 + w_2 + w_3} \quad (1)$$

Where w is the weight fraction of the material and mwt_w is the weighted molecular. In addition, the maximum, minimum, median and the weighted variance of each physical properties was included from each composition. Using the mwt as an example, the values pertaining to the material with the highest, lowest and middle mwt were also recorded for each formulation. The weighted variance of the mwt, for example, was calculated by first determining the weighted average and then subsequently calculating the spread around the weighted average:

$$Weighted\ Variance\ mwt = \frac{w_1 \cdot (mwt_1 - mwt_w)^2 + w_2 \cdot (mwt_2 - mwt_w)^2 + w_3 \cdot (mwt - mwt_w)^2}{w_1 + w_2 + w_3} \quad (2)$$

The final feature was a count of the number of materials per formulation. A representation of the feature set is presented in Table S1–2. The 16 features used were compared with the 3 physical properties features previously used to help enrich the feature set and capture the differences between the 1437 different formulations. The 16 features were scaled and decomposed into 2 dimensions using principal component analysis (PCA) using the *scikit-learn* package (v.0.24.2). This feature set was not used for the training of the model, but to purely visualise the FDM formulation space.

4.4. Experimental validation

4.4.1. Materials

Klucel® EF, Aquasolve® LG, Aquasolve® HG, and Hydroxyethyl cellulose (HEC) Natrosol™ 250H were all purchased from Ashland Inc. (USA). Paracetamol, magnesium stearate, polyethylene oxide (PEO) 8 M, polyethylene glycol (PEG) 8 K, and Kolliphor P407 were purchased from Sigma Aldrich (USA). Mannitol was purchased from Fisher Scientific International Inc. (USA), and Polyox™ WSR 303 was acquired from DDP Specialty Electronic Materials US Inc. (USA).

4.4.2. Hot melt extrusion (HME)

Four AI-generated formulations were experimentally validated, each of which was mixed using a mortar and pestle at specific compositions (Table 1). After being mixed, the samples were loaded onto a single-screw extruder (Noztek Pro-filament extruder, NozteK, UK), and based on specific formulation requirements, extrusion was carried out at a fixed screw speed of 15 rpm through nozzles of different diameters under different temperature conditions. In this way, suitable filaments for printing for each formulation were obtained for subsequent analyses and experiments.

4.4.3. Material characterisation

4.4.3.1. DSC. Differential scanning calorimetry (DSC) was performed to characterise the formulations. DSC measurements were made with a Q20 DSC (TA instruments, Waters LLC, USA). Calibrations for the cell constant and enthalpy were made with indium (T_m=156.6 °C, $\Delta_f H$=28.71 J/g), in accordance with specified manufacturer guidelines. Nitrogen was used as the purge gas, at a flow rate of 50 mL/ min, for all the experiments performed. Tzero aluminium pans and pin-holed hermetic lids (TA instruments, Waters LLC, USA) were used with an average sample mass of 3–5 mg

4.4.3.2. PXRD. Powder X-ray diffraction (PXRD) patterns were acquired using a Rigaku MiniFlex 600 (Rigaku, USA) equipped with a Cu Kα X-ray source (λ = 1.5418 Å) having an intensity of 15 mA and a voltage applied of 40 kV. The angular range of data acquisition was 3 – 40° 2θ, having a stepwise size of 0.02° set at a speed of 2°/min.

4.4.4. 3D printing

The Anycubic Kobra 2 (3D printer, fused-deposition modelling, Anycubic Inc., China) was utilised to create dosage forms. To guarantee optimal printing conditions, a printer nozzle of 0.8 mm was used, and an SLA 3D-printed extrusion gear set with smaller teeth was utilised in place of the original gears to prevent filament grinding, which was more compatible with the soft active pharmaceutical ingredient (API)-loaded filament (Fig. 10). The customised gear set was printed using the Form 2 printer with Clear V4 resin (Formlabs Inc., USA).

For the 3D model design of the dosage forms, Onshape (PTC, USA) software was utilised. The model was subsequently exported as a .stl file for printing preparation in Ultimaker Cura (Ultimaker Inc., USA). The chosen geometry for the AI-generated formulations were tablets with dimensions of $X = 10$ mm, $Y = 10$ mm, and $Z = 3$ mm. The settings for the printer were adjusted accordingly: a 10 % infill percentage was selected, the retraction option was turned off, extrusion temperature ranged between 150 and 210 °C, build plate temperature was adjusted to 60 °C, printing speeds were maintained at 20 mm/s, and the layer height

Fig. 10. The original (left-hand side) and the customised extrusion gear set with smaller gear teeth (right-hand side). The custom extrusion gear set was 3D printed and modified from the original design to help improve printability.

was set to 0.10 mm.

CRediT authorship contribution statement

Moe Elbadawi: Methodology, Investigation, Formal analysis, Data curation, Conceptualization. **Hanxiang Li:** Writing – original draft, Formal analysis, Data curation. **Siyuan Sun:** Data curation. **Manal E. Alkahtani:** Formal analysis, Data curation. **Abdul W. Basit:** Writing – review & editing, Writing – original draft, Supervision, Methodology, Conceptualization. **Simon Gaisford:** Writing – review & editing, Supervision, Conceptualization.

Declaration of competing interest

The authors declare that they have no known competing financial interests or personal relationships that could have appeared to influence the work reported in this paper.

Data availability

Data will be made available on request.

Acknowledgements

M.E. would like to acknowledge the Engineering Physical Science Research Council for their funding support [Grant number: EP/S009000/1]. The authors would like to thank Prince Sattam bin Abdulaziz University, Alkharj, Saudi Arabia, for their financial support of Manal E. Alkahtani through the Postgraduate Research Grant.

Supplementary materials

Supplementary material associated with this article can be found, in the online version, at doi:10.1016/j.apmt.2024.102061.

References

[1] P.K. BG, et al., 3D printing in personalized medicines: A focus on applications of the technology, Materials Today Communications (2023) 105875.
[2] A.J. Capel, et al., 3D printing for chemical, pharmaceutical and biological applications, Nature Reviews Chemistry 2 (12) (2018) 422–436.
[3] S.N. Economidou, D. Douroumis, 3D printing as a transformative tool for microneedle systems: Recent advances, manufacturing considerations and market potential, Advanced Drug Delivery Reviews 173 (2021) 60–69.
[4] Z. Liu, et al., Looking into the future: toward advanced 3D biomaterials for stem-Cell-based regenerative medicine, Advanced Materials 30 (17) (2018) 1705388.
[5] A.P. McCloskey, et al., 3D printing–an alternative strategy for pediatric medicines, 16, Taylor & Francis, 2023, pp. 613–616.
[6] M.E. Prendergast, J.A. Burdick, Recent advances in enabling technologies in 3D printing for precision medicine, Advanced Materials 32 (13) (2020) 1902516.
[7] Q. Yu, et al., The applications of 3D printing in wound healing: the external delivery of stem cells and antibiosis, Advanced Drug Delivery Reviews (2023) 114823.
[8] V.M. Vaz, L. Kumar, 3D printing as a promising tool in personalized medicine, Aaps Pharmscitech 22 (2021) 1–20.
[9] S. Lamichhane, et al., Complex formulations, simple techniques: Can 3D printing technology be the Midas touch in pharmaceutical industry? Asian journal of pharmaceutical sciences 14 (5) (2019) 465–479.
[10] X. Zhu, et al., 3D printing promotes the development of drugs, Biomedicine & Pharmacotherapy 131 (2020) 110644.
[11] W.-K. Hsiao, et al., 3D printing of oral drugs: a new reality or hype? Expert opinion on drug delivery 15 (1) (2018) 1–4.
[12] S. Pravin, A. Sudhir, Integration of 3D printing with dosage forms: A new perspective for modern healthcare, Biomedicine & Pharmacotherapy 107 (2018) 146–154.
[13] M. Elbadawi, et al., Harnessing artificial intelligence for the next generation of 3D printed medicines, Advanced Drug Delivery Reviews 175 (2021) 113805.
[14] S.J. Trenfield, et al., Advancing pharmacy and healthcare with virtual digital technologies, Advanced Drug Delivery Reviews 182 (2022) 114098.
[15] Z. Bao, et al., Revolutionizing Drug Formulation Development: The Increasing Impact of Machine Learning, Advanced Drug Delivery Reviews (2023) 115108.
[16] R.J. Chen, et al., Algorithmic fairness in artificial intelligence for medicine and healthcare, Nature biomedical engineering 7 (6) (2023) 719–742.
[17] M.W. Mullowney, et al., Artificial intelligence for natural product drug discovery, Nature Reviews Drug Discovery (2023) 1–22.
[18] T. DebRoy, et al., Metallurgy, mechanistic models and machine learning in metal printing, Nature Reviews Materials 6 (1) (2021) 48–68.
[19] H. Tao, et al., Nanoparticle synthesis assisted by machine learning, Nature Reviews Materials 6 (8) (2021) 701–716.
[20] Z.F. Greenberg, et al., Towards artificial intelligence-enabled extracellular vesicle precision drug delivery, Advanced Drug Delivery Reviews (2023) 114974.
[21] P. Hassanzadeh, et al., The significance of artificial intelligence in drug delivery system design, Advanced Drug Delivery Reviews 151 (2019) 169–190.
[22] P. Bannigan, et al., Machine learning directed drug formulation development, Advanced Drug Delivery Reviews 175 (2021) 113806.
[23] Y. Abdalla, et al., Machine learning using multi-modal data predicts the production of selective laser sintered 3D printed drug products, International Journal of Pharmaceutics 633 (2023) 122628.
[24] C.S. O'Reilly, et al., Machine learning and machine vision accelerate 3D printed orodispersible film development, Pharmaceutics 13 (12) (2021) 2187.
[25] F. Wang, et al., Machine learning predicts electrospray particle size, Materials & Design 219 (2022) 110735.
[26] H. Bennett-Lenane, et al., Machine learning methods for prediction of food effects on bioavailability: A comparison of support vector machines and artificial neural networks, European Journal of Pharmaceutical Sciences 168 (2022) 106018.
[27] H.Y. Jang, et al., Machine learning-based quantitative prediction of drug exposure in drug-drug interactions using drug label information, NPJ Digital Medicine 5 (1) (2022) 88.
[28] M. Ficzere, et al., Real-time coating thickness measurement and defect recognition of film coated tablets with machine vision and deep learning, International Journal of Pharmaceutics 623 (2022) 121957.
[29] M. Ficzere, et al., Image-based simultaneous particle size distribution and concentration measurement of powder blend components with deep learning and machine vision, European Journal of Pharmaceutical Sciences (2023) 106611.
[30] C. Wang, et al., Prediction of enhanced drug solubility related to clathrate compositions and operating conditions: Machine learning study, International Journal of Pharmaceutics 646 (2023) 123458.
[31] F. Wang, et al., Advancing oral delivery of biologics: Machine learning predicts peptide stability in the gastrointestinal tract, International Journal of Pharmaceutics 634 (2023) 122643.
[32] Y. Hayashi, et al., Application of unsupervised and supervised learning to a material attribute database of tablets produced at two different granulation scales, International Journal of Pharmaceutics 641 (2023) 123066.
[33] A. Zhang, et al., Shifting machine learning for healthcare from development to deployment and from models to data, Nature biomedical engineering 6 (12) (2022) 1330–1345.
[34] A. Lamiable, et al., Revealing invisible cell phenotypes with conditional generative modeling, Nature Communications 14 (1) (2023) 6386.
[35] S. Hussain, et al., High-content image generation for drug discovery using generative adversarial networks, Neural Networks 132 (2020) 353–363.
[36] A. Gupta, J. Zou, Feedback GAN for DNA optimizes protein functions, Nature Machine Intelligence 1 (2) (2019) 105–111.
[37] O. Méndez-Lucio, et al., De novo generation of hit-like molecules from gene expression signatures using artificial intelligence, Nature Communications 11 (1) (2020) 10.
[38] S.K.J. Rizvi, et al., Spectrum of advancements and developments in multidisciplinary domains for generative adversarial networks (GANs), Archives of Computational Methods in Engineering (2021) 1–19.
[39] S. Kazeminia, et al., GANs for medical image analysis, Artificial Intelligence in Medicine 109 (2020) 101938.
[40] S. Chun, et al., Deep learning for synthetic microstructure generation in a materials-by-design framework for heterogeneous energetic materials, Scientific reports 10 (1) (2020) 13307.
[41] A.M. Mroz, et al., Into the Unknown: How Computation Can Help Explore Uncharted Material Space, Journal of the American Chemical Society 144 (41) (2022) 18730–18743.
[42] G. Chen, et al., Machine-learning-assisted de novo design of organic molecules and polymers: Opportunities and challenges, Polymers 12 (1) (2020) 163.
[43] X. Han, et al., ProGAN: Protein solubility generative adversarial nets for data augmentation in DNN framework, Computers & Chemical Engineering 131 (2019) 106533.
[44] A. Zhavoronkov, et al., Will artificial intelligence for drug discovery impact clinical pharmacology? Clinical Pharmacology & Therapeutics 107 (4) (2020) 780–785.
[45] A. Kadurin, et al., druGAN: an advanced generative adversarial autoencoder model for de novo generation of new molecules with desired molecular properties in silico, Molecular pharmaceutics 14 (9) (2017) 3098–3104.
[46] A. Zhavoronkov, et al., Potential 2019-nCoV 3C-like protease inhibitors designed using generative deep learning approaches, ChemRxiv (2020), https://doi.org/10.26434/chemrxiv.11829102.v2. Cambridge: Cambridge Open Engage.
[47] P.A.M. Zapata, et al., Cell morphology-guided de novo hit design by conditioning GANs on phenotypic image features, Digital Discovery 2 (1) (2023) 91–102.
[48] M. Skalic, et al., Shape-based generative modeling for de novo drug design, Journal of chemical information and modeling 59 (3) (2019) 1205–1214.
[49] X. Zeng, et al., Deep generative molecular design reshapes drug discovery, Cell Reports Medicine (2022).
[50] M. Ragoza, et al., Generating 3D molecules conditional on receptor binding sites with deep generative models, Chemical science 13 (9) (2022) 2701–2713.

[51] M. Karimi, et al., De novo protein design for novel folds using guided conditional Wasserstein generative adversarial networks, Journal of chemical information and modeling 60 (12) (2020) 5667–5681.
[52] Y. Dan, et al., Generative adversarial networks (GAN) based efficient sampling of chemical composition space for inverse design of inorganic materials, NPJ Computational Materials 6 (1) (2020) 84.
[53] C.T. Chen, G.X. Gu, Generative deep neural networks for inverse materials design using backpropagation and active learning, Advanced Science 7 (5) (2020) 1902607.
[54] H. Türk, et al., Assessing deep generative models in chemical composition space, Chemistry of Materials 34 (21) (2022) 9455–9467.
[55] Y. Dong, et al., Inverse design of two-dimensional graphene/h-BN hybrids by a regressional and conditional GAN, Carbon 169 (2020) 9–16.
[56] K. Zhou, et al., Deep convolutional generative adversarial network with semi-supervised learning enabled physics elucidation for extended gear fault diagnosis under data limitations, Mechanical Systems and Signal Processing 185 (2023) 109772.
[57] W. Li, et al., Tackling mode collapse in multi-generator GANs with orthogonal vectors, Pattern Recognition 110 (2021) 107646.
[58] B. Yilmaz, R. Korn, Synthetic demand data generation for individual electricity consumers: Generative Adversarial Networks (GANs), Energy and AI 9 (2022) 100161.
[59] D. Saxena, J. Cao, Generative adversarial networks (GANs) challenges, solutions, and future directions, ACM Computing Surveys (CSUR) 54 (3) (2021) 1–42.
[60] S. Durr, et al., Effective dynamics of generative adversarial networks, Physical Review X 13 (4) (2023) 041004.
[61] A. Isreb, et al., 3D printed oral theophylline doses with innovative 'radiator-like' design: Impact of polyethylene oxide (PEO) molecular weight, International Journal of Pharmaceutics 564 (2019) 98–105.
[62] M. Elbadawi, et al., 3D printing tablets: Predicting printability and drug dissolution from rheological data, International Journal of Pharmaceutics 590 (2020) 119868.
[63] National Academies of Sciences, E. and Medicine, Reproducibility and Replicability in Science, The National Academies Press, Washington, DC, 2019.
[64] S.M. Ritter, A. Dijksterhuis, Creativity—the unconscious foundations of the incubation period, Frontiers in human neuroscience 8 (2014) 215.
[65] L.E. McCoubrey, et al., Active machine learning for formulation of precision probiotics, International Journal of Pharmaceutics 616 (2022) 121568.
[66] K.E. Ak, et al., Semantically consistent text to fashion image synthesis with an enhanced attentional generative adversarial network, Pattern Recognition Letters 135 (2020) 22–29.
[67] Choshen, L., et al. (2019). "On the weaknesses of reinforcement learning for neural machine translation." arXiv preprint arXiv:1907.01752.
[68] A. Borji, Pros and cons of gan evaluation measures, Computer vision and image understanding 179 (2019) 41–65.
[69] I. Goodfellow, et al., Generative adversarial networks, Communications of the ACM 63 (11) (2020) 139–144.
[70] M. Arjovsky, et al., Wasserstein Generative Adversarial Networks, in: P. Doina, T. Yee Whye (Eds.), Proceedings of the 34th International Conference on Machine Learning, Proceedings of Machine Learning Research, PMLR. 70, 2017, pp. 214–223.
[71] Shi, M., et al. (2023). "Cutout with patch-loss augmentation for improving generative adversarial networks against instability." Computer vision and image understanding: 103761.
[72] L. Feng, et al., CRPGAN: Learning image-to-image translation of two unpaired images by cross-attention mechanism and parallelization strategy, Plos one 18 (1) (2023) e0280073.
[73] C. Wang, et al., An adversarial model for electromechanical actuator fault diagnosis under nonideal data conditions, Neural Computing and Applications (2022) 1–22.
[74] A. Goyanes, et al., PET/CT imaging of 3D printed devices in the gastrointestinal tract of rodents, International Journal of Pharmaceutics 536 (1) (2018) 158–164.
[75] S. Ayyoubi, et al., 3D printed, personalized sustained release cortisol for patients with adrenal insufficiency, International Journal of Pharmaceutics 630 (2023) 122466.
[76] M. DeCamp, C. Lindvall, Mitigating bias in AI at the point of care, Science 381 (6654) (2023) 150–152.
[77] R. Challen, et al., Artificial intelligence, bias and clinical safety, BMJ Quality & Safety 28 (3) (2019) 231–237.
[78] G. Harshvardhan, et al., A comprehensive survey and analysis of generative models in machine learning, Computer Science Review 38 (2020) 100285.
[79] B.M. Castro, et al., Machine learning predicts 3D printing performance of over 900 drug delivery systems, Journal of Controlled Release 337 (2021) 530–545.
[80] M. Elbadawi, et al., M3DISEEN: A novel machine learning approach for predicting the 3D printability of medicines, International Journal of Pharmaceutics 590 (2020) 119837.